# Design and Verification of Parallelogram Mechanism With Geared Unit Rolling Joints for Reliable Wiring

Jungwook Suh, *Member, IEEE*, and Wontae Choi

***Abstract*—The structure of 1-DOF joints used in existing robots is generally a revolute or a prismatic joint. However, recently, attempts have been made to apply rolling joints to reduce the size and weight of surgical and humanoid robots. In this study, to take advantages of wire routing through robot joints, a new method for applying geared rolling units to a parallelogram mechanism is proposed. First, a kinematic analysis of the proposed gear-based mechanism is explained in comparison with the existing pivot-based mechanism. In addition, the importance of the radii of the gears is verified through force analysis to prevent damage to the applied gears, as well as through the analysis of actuation torque and singular positions, in which the parallelogram can convert into an anti-parallelogram. The effect of stable wiring was verified through an experiment using a cable-driven prototype. Consequently, the proposed parallelogram mechanism composed of rolling units is expected to be applied to various robot configurations owing to its advantages.**

***Index Terms*—Mechanism design, actuation and joint mechanisms, tendon/wire mechanism, kinematics.**

## I. Introduction

IN SEVERAL industrial robot arms, a motor for generating torque is directly connected to the joint axis. This motor usually includes a reducer that amplifies the torque and an encoder that measures the rotation angle. If a motor controller is located on the base part, several strands of electrical wire are required to transmit the motor power and sensor signals. On the other hand, even if the motor controller is placed in the joint part together with the motor, wiring is required for communication and power supply. A robot is generally composed of multiple joints that enable it to implement various motions through reprogramming. In a serial robot with the motors structurally connected to the joint directly, the wiring of the motor located at the distal part must pass through all other joints; further, the joint located at the proximal part should provide enough space to other motors for wiring.

Existing methods for protecting electrical wires, which transmit power and signals to motors and sensors located at the distal end of the proximal joints of the robot arm, can be classified into three categories as follows:

1) Dress pack: Wires are routed to the outside of the joints using a hose-type protection tube. It can be easily used for a simple assembly in the case of wiring correction. However, it requires additional space outside the robot and can be damaged by wear. Furthermore, the shape of the dress pack is difficult to predict as it changes with the posture change of the robot. Therefore, there is a possibility of collision with the robot's surroundings [1], [2].
2) Hollow joint: A motor with a hollow shaft at the center of rotation is applied to the joint, and distally connected wires are placed inside the joint hollow. Currently, this is one of the most widely used methods for robotic arms composed of revolute joints. This enables neat wiring, but it is difficult to modify the wiring using this method. In addition, the structure of the speed reducer and sensor is limited to the hollow type of the motor, which can increase the hardware cost [3], [4], [5].
3) Slip ring: Power and signals are transmitted using brushes that maintain continuous contact during the rotational motion of a joint. Infinite rotation is a significant advantage, and recently, slip rings have been used for high-frequency signal transmission and optical communication. However, increasing the number of wires also increases the cost of the components, as well as the difficulty in designing the joints [6], [7].

Each of the three conventional wiring methods has distinct advantages and disadvantages. At present, it is difficult to find a method that offers the advantages of stable wire protection with predictable shape during joint movement, while allowing for free wiring modification at a low cost. This can be attributed to the structural limit of the conventional pivot joint, in which a relative one-degree-of-freedom (DOF) rotational motion between two adjacent links occurs about a single axis.

Unlike the pivot joint, a rolling joint can have 1-DOF motion about two consecutive rotational axes in the form of a polycentric or multi-axial joint, similar to a gear pair. Joints based on rolling motion have mainly been developed for application to miniature robot arms, such as surgical robots [8], [9], [10]. Recently, rolling joints have been applied to reduce the weight of humanoid robots [11], [12], [13]. A significant feature of the cable-driven rolling joint is that the distal joint is not affected by the movement of the joint located in the middle [14]. Using this feature, the motion of the rolling joints may not affect the properly aligned electrical wires. As a result, reliable protection of the wires can be ensured and their predictable deformation will not constrain the movement of the robot.

In this study, a new method for applying rolling joints is proposed for the advantage of wiring in the joints of robots. To

Manuscript received 2 October 2022; accepted 16 March 2023. Date of publication 5 April 2023; date of current version 9 May 2023. This letter was recommended for publication by Associate Editor X. Kong and Editor J. Desai upon evaluation of the reviewers' comments. This work was supported in part by the National Research Foundation of Korea (NRF) under Grant NRF-2020R1C1C1008707 and in part by the Institute of Information and communications Technology Planning and Evaluation (IITP) under Grant 2022-0-00501, and project BK21 FOUR funded by the Korea government (MSIT). *(Corresponding author: Jungwook Suh.)*

The authors are with the Department of Robot and Smart System Engineering, Kyungpook National University, Daegu 41566, South Korea (e-mail: jwsuh@knu.ac.kr; wtchoi@knu.ac.kr).

Digital Object Identifier 10.1109/LRA.2023.3264716

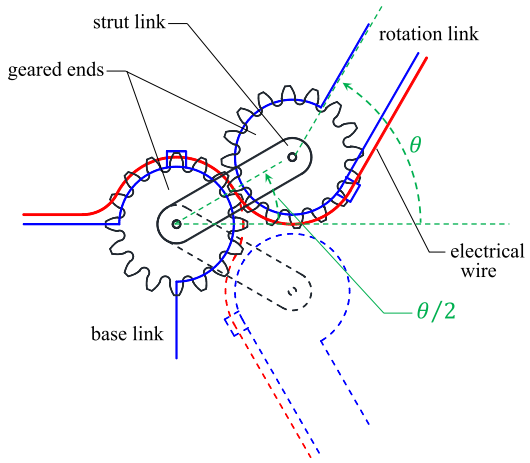


Fig. 1. Schematic diagram of a geared rolling joint with electrical wiring.

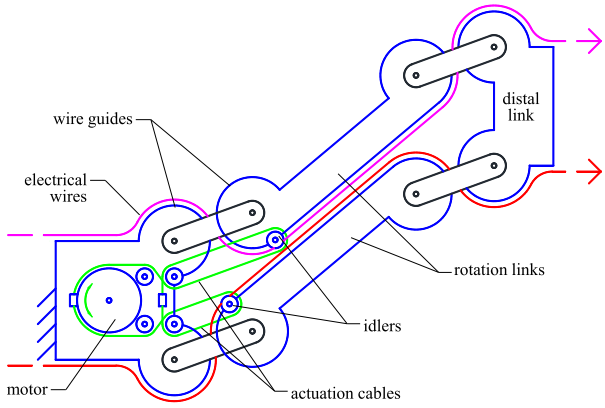


Fig. 2. Proposed parallelogram mechanism with geared rolling units.

verify the effectiveness of the proposed joint, a parallel four-bar linkage consisting of gear-based unit rolling joints is used. The remainder of this letter is organized as follows. The unit rolling joint for wiring is explained in Section II. The kinematic position of a parallelogram mechanism with rolling units is analyzed in Section III. Section IV presents a force analysis along with the singularities of this mechanism. Section V presents the design and manufacture of the prototype of the proposed parallelogram, and in Section VI, the experimental tests are discussed. Finally, the conclusions are summarized in Section VII.

## II. Rolling-Based Parallelogram

The unit rolling joint, a basic component of the new parallel four-bar linkage proposed in this study, is configured as shown in Fig. 1. The blue lines show base and rotation links, including wire guides, whereas the red line shows the electrical wires. Circular spur gears can be applied to prevent slipping on rolling surfaces, and wire guides can be placed on the side of the gears. Unlike the general pivot joint that rotates about an axis, the unit rolling joint of the proposed mechanism has two rotation axes, constrained by the gears to have a 1-DOF motion. The electrical wire passing through the joint was partially wound and aligned along the cylindrical guides located on the side of the gears, and the winding angle of the wire was changed by the rotation of the joint. Even if the wire is partially fixed to the guide, it does not interfere with the rotary link motion. The angle of the strut link, keeping the distance between the two gears constant, is half the angle of the rotation link. Therefore, the proposed mechanism corresponds to a nonconvex octagon with reflex angles rather than a quadrilateral.

In this study, to confirm that a gear-based rolling joint can provide a stable wiring route, a parallelogram using gear-based rolling units was utilized. Parallelograms are commonly used in palletizing robots to handle large payloads, allowing the construction of a low-DOF robot arm that limits the orientation of the distal end. Energy efficiency can also be improved by placing the actuators for the pitching joints closer to the base part. Thus, parallelograms have been widely used for their structural advantages for a long time, but the basic structure composed of pivot unit joints has not changed.

Fig. 2 shows the conceptual structure of the new parallelogram mechanism proposed in this study. The angle of the two long rotation links located in the center changes with respect to the fixed base link on the lower left; as a result, the position of the distal link on the upper right changes with a fixed orientation. Unlike conventional parallelogram mechanisms, a unit joint formed by joining two of the four main links performs a 1-DOF rolling motion. The clockwise rotational motion of the motor pulls the lower actuation cable to generate a counterclockwise rotational motion on the lower long rotation link. The electrical wires starting at the base link are aligned along the wire guides of the rolling joints and run toward the end link. The wires are fixed on each link such that the relative position does not change; as a result, stable wiring can be provided regardless of the parallelogram motion.

We can predict that the proposed mechanism composed of four geared unit joints will have a 1-DOF motion, similar to the general parallelogram. The DOF of the planal mechanisms can be analyzed by applying Kutzbach's formula: $M = 3(N-1) - 2J_1 - J_2$ (where $N$ = number of links, $J_1$ = number of 1-DOF joints, and $J_2$ = number of 2-DOF joints). If the actuation cables are not considered in this problem, the number of links, including the short strut links between the gears, is $N = 8$. Here, the number of 1-DOF joints is equal to the number of gears, and the number of 2-DOF joints is the same as the number of geared rolling units: $J_1 = 8$, $J_2 = 4$. Therefore, the DOF of the proposed parallelogram is confirmed to be $M = 1$, as predicted. In this mechanism, the rotation angle provided by a motor can determine its posture.

Unlike general pivot joints, the center of rotation of a rolling joint is not defined as a single axis. Therefore, a parallelogram composed of rolling units requires a special actuation mechanism. The following methods are considered, as shown in Fig. 3.

1) Rotation of strut link: Rotating the short strut link between two gears can drive the rotation link. Because the rolling joint acts as a 1:2 accelerator, a relatively large motor torque is required to drive the rolling-based mechanism.
2) Rotation of the ring gear: If a planetary gear train is configured by applying an additional ring gear, the parallelogram can be rotated by driving the ring gear. A ring gear with a large diameter can cause a loss in terms of cost and space.
3) Tendon actuation: Tendon actuation using a cable-like transmission can be applied to one or several rolling joints in Fig. 3(c). In some cases, the inner space between the upper and lower rolling units can be utilized, as also shown in Fig. 3(d).

To construct a palletizing robot, the last method is a reasonable choice without loss of torque while saving space. Meanwhile,

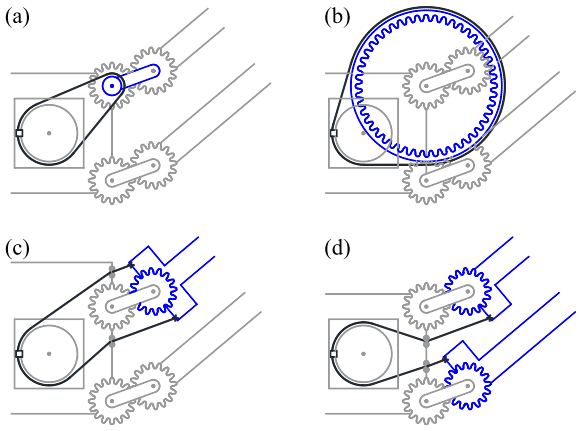


Fig. 3. Methods for driving the rolling-based parallelogram: applying torque (a) on a strut link, (b) on a rotation link via an additional ring gear, (c) on a rotation link using tendons, and (d) on both rotation links using tendons.

TABLE I
DH PARAMETERS FOR PIVOT-BASED PARALLELOGRAM

| $i$ | $a_{i-1}$ | $\alpha_{i-1}$ | $d_i$ | $\theta_i$ |
|---|---|---|---|---|
| 1 | - | - | - | $\theta$ |
| 2 | $L_\mathrm{J}$ | - | - | $-\theta$ |

TABLE II
DH PARAMETERS FOR ROLLING-BASED PARALLELOGRAM

| $i$ | $a_{i-1}$ | $\alpha_{i-1}$ | $d_i$ | $\theta_i$ |
|---|---|---|---|---|
| 1 | - | - | - | $\theta/2$ |
| 2 | $2R_\mathrm{J}$ | - | - | $\theta/2$ |
| 3 | $L_\mathrm{J}$ | - | - | $-\theta/2$ |
| 4 | $2R_\mathrm{J}$ | - | - | $-\theta/2$ |

the limited elasticity of the actuation tendon can be improved by winding around multiple idlers.

## III. KINEMATIC ANALYSIS

### A. Joint Space and Task Space

The kinematics of a parallelogram linkage composed of conventional pivot units can be represented using two sets of Denavit-Hartenberg (DH) parameters because of the characteristics of the parallel mechanism in which the angle of the distal link is maintained. Table I lists the DH parameters of the conventional parallelogram according to Craig's modified method [15]. On the other hand, the proposed parallelogram is relatively more complicated by the additional gears. Its kinematics can be expressed as four sets of DH parameters, as shown in Table II [16], [17]. Here, $L_\mathrm{J}$ is a constant representing the length of the long rotation links, and $\theta$ is a variable representing the rotation angle of the rotation links. $R_\mathrm{J}$ represents the radius of the gear pitch circle. It is assumed that the strut links are horizontal as are the actuation links in the neutral position.

Fig. 4 shows the local coordinate systems attached to each link for kinematic analysis of the proposed rolling-based parallelogram. The kinematics of this mechanism can be expressed

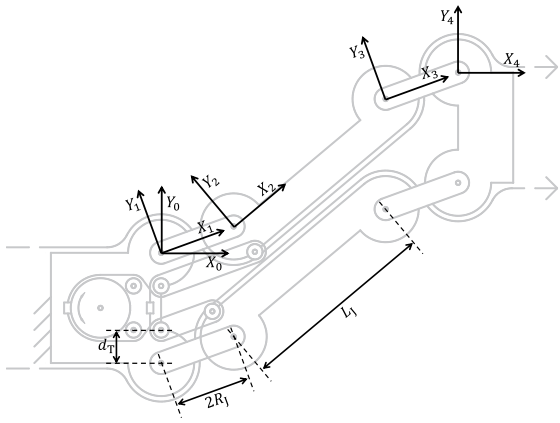


Fig. 4. Coordinate systems of the proposed parallelogram.

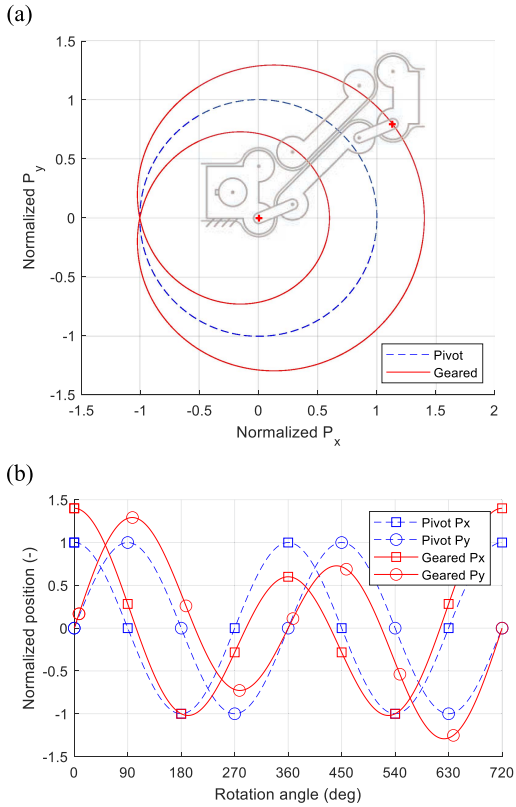


Fig. 5. Position change of the distal link by applying the unit rolling joints.

using a transformation matrix as follows:

$$ {}^{0}_{4}T = \begin{bmatrix} 1 & 0 & 0 & L_\mathrm{J}\cos\theta + 4R_\mathrm{J}\cos\frac{\theta}{2} \\ 0 & 1 & 0 & L_\mathrm{J}\sin\theta + 4R_\mathrm{J}\sin\frac{\theta}{2} \\ 0 & 0 & 1 & 0 \\ 0 & 0 & 0 & 1 \end{bmatrix} \tag{1} $$

From (1), the rotation matrix always has the form of an identity matrix regardless of the radius of the rolling surface $R_\mathrm{J}$. Therefore, the orientation of the distal link is always kept constant, such as in the existing parallelogram mechanisms.

From the fourth column of (1), the position of the distal link is affected by $R_\mathrm{J}$ and differs from pivot-based mechanisms, and without consideration of singularities, as also shown in Fig. 5. The blue dotted lines show the case of $R_\mathrm{J}/L_\mathrm{J} = 0$, while the

red solid lines show $R_{\mathrm{J}}/\,L_{\mathrm{J}} = 0.1$. In Fig. 5(b), the square and circular markers represent the x-axis and y-axis coordinates, respectively. Notably, the distal position of the geared mechanism repeats with a period of 720°. Thus, intuitively, the x-axis position changes to $L_{\mathrm{J}} + 4R_{\mathrm{J}},\ L_{\mathrm{J}} - 4R_{\mathrm{J}},$ and $L_{\mathrm{J}} + 4R_{\mathrm{J}}$ for rotation angles $\theta$ is $0,\ 360,$ and $720°$, respectively.

### B. Motor Space and Joint Space

By applying multiple idlers to the rolling-based joints of the cable-actuated robot, the actuation cable can be wound around the idlers $N_{\mathrm{C}}$ times to perform the role of a $2N_{\mathrm{C}}:1$ speed reducer [11]. Ignoring the size of the idlers away from the center of the gears by $d_{\mathrm{T}}$, the cable length $L_{\mathrm{C}}$ for rotating the rolling joint by an angle $\theta$ is as follows:

$$L_{\mathrm{C}} = 4N_{\mathrm{C}}\left(R_{\mathrm{J}} + d_{\mathrm{T}}\sin\frac{\theta}{2}\right) \tag{2}$$

Even if the radius of the idlers is large, this relation is valid because the partial length of the cable wound around the idlers is always constant. Therefore, based on the neutral posture with $\theta = 0°$, the actuation length of the cable $\Delta L_{\mathrm{C}}$ is

$$\Delta\, L_{\mathrm{C}} = 4N_{\mathrm{C}}d_{\mathrm{T}}\sin\frac{\theta}{2} \tag{3}$$

Using the radius $R_{\mathrm{M}}$ of the actuation spool coupled to the motor and rotation angle $\theta_{\mathrm{M}}$ of the motor, the cable actuation length can be calculated as follows:

$$\Delta\, L_{\mathrm{C}} = \theta_{\mathrm{M}}\, R_{\mathrm{M}} \tag{4}$$

Summarizing (3), (4), the joint angle can be expressed using the motor angle as follows:

$$\theta = 2\sin^{-1}\frac{\theta_{\mathrm{M}}R_{\mathrm{M}}}{4N_{\mathrm{C}}d_{\mathrm{T}}} \tag{5}$$

Therefore, the motor and joint angles have a nonlinear relationship. The smaller the diameter of the actuation spool and the farther the idlers are placed from the center of the gears, the higher the reduction ratio, which is maximized at $\theta = 0°$, such that a large joint torque can be generated. However, when gravity is applied in the direction of the $\mathrm{Y}_4$-axis on the distal link, the moment arm is maximized at $\theta = 0°$, and the payload of the mechanism is determined.

## IV. Force Analysis & Singularities

### A. Force Analysis

The proposed parallelogram uses gears to implement rolling motion in unit joints. Therefore, it is necessary to examine the load and resultant damage to the components of the mechanism such as gears and strut links. First, when a force and moment are applied to the distal link, the torque transmitted to the gears required to maintain the posture statically is calculated. A pair of gear ends of link $i$ and link $j$ constituting a unit gear joint exchange two types of forces. The direction of the normal force $\mathbf{f}_{ij\mathrm{N}}$ applied to the gear tooth surface is determined by the pressure angle of the gears, and the other force $\mathbf{f}_{ij\mathrm{S}}$, applied to the center of the gear through the strut links, is always directed toward the center of the gear in contact.

Fig. 6 shows the force parameters for maintaining a vertically static posture when a force and moment is applied. The link numbers are 0 and 2 for the proximal base link and distal link, respectively, and 1 and 3 for the upper and lower rotation links, respectively. The center of gravity of each link is assumed to be located at the center of both end gears and that the friction and

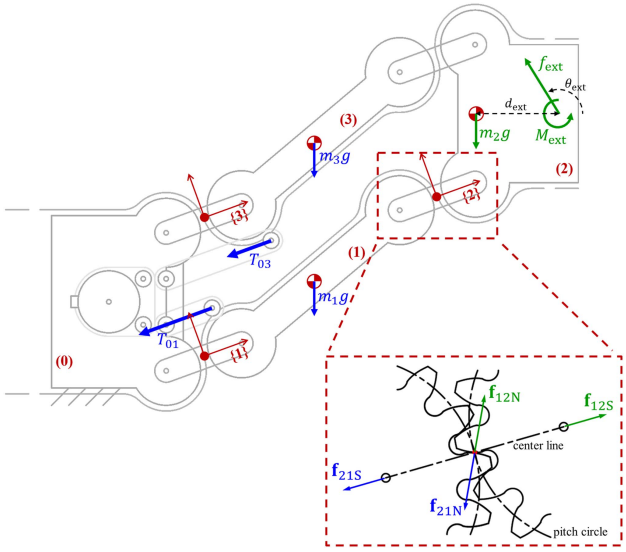


Fig. 6. Forces on the rolling-based parallelogram: blue forces for links (1) and (3) and green forces for links (0) and (2).

weight of the strut links are negligible. The coordinate systems fixed to the links except for link 0 are defined at the contact position of the two gears, and the x-axis of each coordinate system coincides with the longitudinal direction of the strut links.

First of all, the net force applied to the lower rotation link (1) is as follows.

$$\mathbf{F}_1 = \mathbf{f}_{01\mathrm{N}} + \mathbf{f}_{01\mathrm{S}} + \mathbf{f}_{21\mathrm{N}} + \mathbf{f}_{21\mathrm{S}} + \mathbf{T}_{01} + m_1\mathbf{g} \tag{6}$$

Here, $\mathbf{f}_{01\mathrm{N}}$ and $\mathbf{f}_{21\mathrm{N}}$ represent the normal forces exerted on the gear ends of the link (1) by the links (0) and (2), respectively. $\mathbf{f}_{01\mathrm{S}}$ and $\mathbf{f}_{21\mathrm{S}}$ represent forces exerted on the link (1) by the links (0) and (2) through the strut links, respectively. On the other hand, the moment applied to the link (1) is expressed as

$$\begin{aligned} M_{1Z} = {} & \mathbf{P}_{f21N} \times \mathbf{f}_{21\mathrm{N}} + \mathbf{P}_{f21S} \times \mathbf{f}_{21\mathrm{S}} \\ & + \mathbf{P}_{T01} \times \mathbf{T}_{01} + m_1\mathbf{P}_g \times \mathbf{g} \end{aligned} \tag{7}$$

Here, vectors $\mathbf{P}$ represent the position where each force is applied, for example, $\mathbf{P}_{f21S}$ means the position of the applied force $\mathbf{f}_{21\mathrm{S}}$ with respect to the frame $\{2\}$. $m_1$ and g represent the weight of the link and gravitational acceleration, respectively. $\mathbf{T}_{01}$ is the tension of the actuation cable, including the effect of the reciprocating winding. Similarly, the net force and moment applied to the upper rotation link (3) can be calculated as follows:

$$\mathbf{F}_3 = \mathbf{f}_{03\mathrm{N}} + \mathbf{f}_{03\mathrm{S}} + \mathbf{f}_{23\mathrm{N}} + \mathbf{f}_{23\mathrm{S}} + \mathbf{T}_{03} + m_3\mathbf{g} \tag{8}$$

$$\begin{aligned} M_{3Z} = {} & \mathbf{P}_{f23N} \times \mathbf{f}_{23\mathrm{N}} + \mathbf{P}_{f23S} \times \mathbf{f}_{23\mathrm{S}} \\ & + \mathbf{P}_{T03} \times \mathbf{T}_{03} + m_3\mathbf{P}_g \times \mathbf{g} \end{aligned} \tag{9}$$

On the other hand, for the distal link (2), the external force $\mathbf{f}_{\mathrm{ext}}$ and moment $M_{\mathrm{ext}}$ are additionally applied at a distance of $d_{\mathrm{ext}}$ horizontally from the center of gravity. Using reaction forces ($\mathbf{f}_{ji\mathrm{N}} = -\mathbf{f}_{ij\mathrm{N}},\ \mathbf{f}_{ji\mathrm{S}} = -\mathbf{f}_{ij\mathrm{S}}$) applied by links (1) and (3), the inertial force and moment applied to the distal link are calculated as follows:

$$\mathbf{F}_2 = \mathbf{f}_{12\mathrm{N}} + \mathbf{f}_{12\mathrm{S}} + \mathbf{f}_{32\mathrm{N}} + \mathbf{f}_{32\mathrm{S}} + m_2\mathbf{g} + \mathbf{f}_{\mathrm{ext}} \tag{10}$$

$$\begin{aligned} M_{2Z} = {} & \mathbf{P}_{f12N} \times \mathbf{f}_{12\mathrm{N}} + \mathbf{P}_{f32S} \times \mathbf{f}_{32\mathrm{S}} \\ & + m_2\mathbf{P}_g \times \mathbf{g} + \mathbf{P}_{fext} \times \mathbf{f}_{\mathrm{ext}} + M_{\mathrm{ext}} \end{aligned} \tag{11}$$

To simplify the calculation, we can assume that the external force is caused by an additional weight and there is no external moment: ${}^0\mathbf{f}_{\text{ext}} = m_{\text{ext}}\mathbf{g},\ M_{\text{ext}} = 0$..

In a situation where the posture is maintained statically, the net forces and moments on the left-hand sides in (6)–(11) are all zero. The tension in the lower actuation cable $\mathbf{T}_{01}$ generates a counterclockwise torque, and another tension $\mathbf{T}_{03}$ is required for the upper actuation cable to prevent cable slack. As a result, we can get becomes a problem of nine simultaneous equations to find nine unknowns, and it can be expressed in a vector-matrix form as follows. (12) shown at the bottom of this page.

In this relation, all values on the left-hand side are given, $f_{ij\text{S}}$, $f_{ij\text{N}}$ and $T_{ij}$ represent the magnitude of the forces $\mathbf{f}_{ij\text{S}}$, $\mathbf{f}_{ij\text{N}}$ and $\mathbf{T}_{ij}$, respectively. And new parameters are adopted to simplify the representation of the matrix: $\text{s}_\theta = \sin\theta$, $\text{c}_\theta = \cos\theta$ and $C = -2R_\text{J}\text{c}_\phi - L_\text{J}\text{c}_{\phi+\theta/2}$.

This problem can be solved sequentially as follows: First, the magnitude of the two forces $\mathbf{f}_{23\text{S}}$ and $\mathbf{f}_{23\text{N}}$ applied to the upper-right gear joint can be obtained simultaneously from the following relationship:

$$\begin{bmatrix} f_{23\text{S}} \\ f_{23\text{N}} \end{bmatrix} = \begin{bmatrix} d_\text{L}\text{c}_{\theta/2} & d_\text{L}\text{s}_{\phi-\theta/2} \\ L_\text{J}\text{s}_{\theta/2} & C \end{bmatrix}^{-1} \times \begin{bmatrix} (m_2+m_{\text{ext}})\, gR_\text{J}\text{c}_{\theta/2} + m_{\text{ext}}gd_{\text{ext}} \\ \|\mathbf{T}_{03}\| d_\text{T}\text{c}_{\theta/2} + m_3 g\left(R_\text{J}\text{c}_{\theta/2} + \frac{L_\text{J}}{2}\text{c}_\theta\right) \end{bmatrix} \tag{13}$$

Next, other forces applied to the upper-left and lower-right gear joints can be sequentially obtained as follows:

$$f_{21\text{N}} = (m_2+m_{\text{ext}})\ g\text{c}_{\theta/2}\text{c}_\phi^{-1} - f_{23\text{N}} \tag{14}$$

$$f_{21\text{S}} = (m_2+m_{\text{ext}})\ g\text{s}_{\theta/2} - f_{23\text{S}} - \text{s}_\phi\left(f_{21\text{N}} + f_{23\text{N}}\right) \tag{15}$$

$$f_{03\text{N}} = c_\phi^{-1}\, m_3 g\text{c}_{\theta/2} + f_{23\text{N}} \tag{16}$$

$$f_{03\text{S}} = T_{03}\ + m_3 g\text{s}_{\theta/2} + f_{23\text{S}} - \text{s}_\phi\left(f_{03\text{N}} - f_{23\text{N}}\right) \tag{17}$$

Then, the other forces on the lower-left joint can be calculated.

$$f_{01\text{N}} = \text{c}_\phi^{-1}\, m_1 g\text{c}_{\theta/2} + f_{21\text{N}} \tag{18}$$

$$f_{01\text{S}} = m_1\ g\text{s}_{\theta/2} + f_{21\text{S}} + T_{01} - \text{s}_\phi\left(f_{01\text{N}} - f_{21\text{N}}\right) \tag{19}$$

Fig. 7 shows an example of the change in the normal forces applied to the gears according to the rotation link angle. If the driving range of the rotation link is limited to $[-90°,\ 90°]$, the maximum normal force on the gears is $f_{01\text{N}} = 28.57$ N when $\theta = -90$ deg, and this value is independent of the radius of the gears $R_J$.

Meanwhile, the tension of the lower actuation cable $T_{01}$ required to maintain the posture of the parallelogram can be obtained using (14), (15).

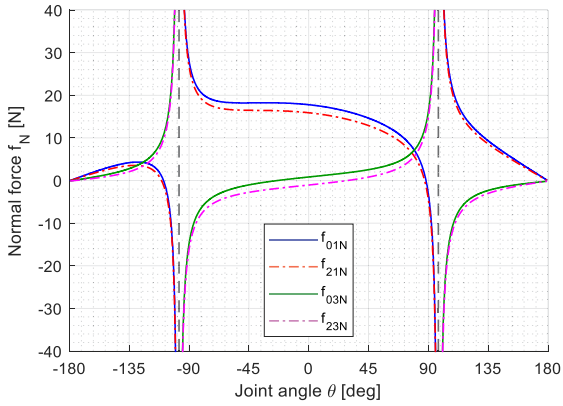


Fig. 7. Normal forces on the gears for vertical actuation: $L_\text{J} = 300$, $R_\text{J} = 30$, $d_\text{L} = 100$, $d_\text{T} = 40$, $d_{\text{ext}} = 0$, $R_\text{M} = 25$ (mm), $\phi = 20$ deg, $T_{03} = 0$, $N_\text{C} = 2$ and $m_1 = m_3 = 0.18$, $m_2 = 0.14$, $m_{\text{ext}} = 1.0$ (kg).

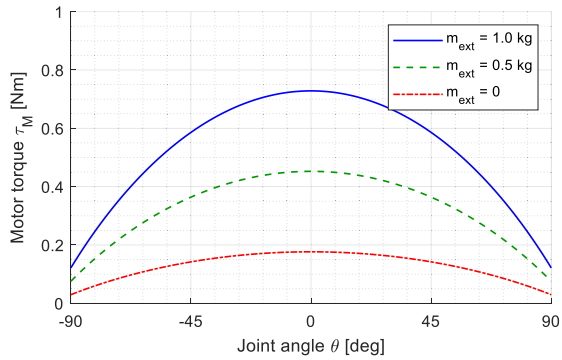


Fig. 8. Required motor torque for vertical actuation with external weight.

$$T_{01} = \frac{1}{d_\text{T}\text{c}_{\theta/2}}\left(m_1 g\left(R_\text{J}\text{c}_{\theta/2} + L_\text{J}\text{c}_\theta/2\right) - f_{21\text{N}}C - f_{21\text{S}}L_\text{J}\text{s}_{\theta/2}\right) \tag{20}$$

The required torque of the motor can be calculated by

$$\tau_\text{M} = \frac{R_\text{M}}{2N_\text{C}}\ (T_{01} - T_{03}) \tag{21}$$

Eventually, substituting (16) into (21), the statically required motor torque is organized as:

$$\tau_\text{M} = \frac{R_\text{M} g}{2N_\text{C} d_\text{T}}\left(\frac{L_\text{J}\text{c}_\theta}{2\text{c}_{\theta/2}} + R_\text{J}\right)(m_1 + 2m_2 + m_3 + 2m_{\text{ext}}) \tag{22}$$

Fig. 8 shows the effect of the external weight $m_{\text{ext}}$ applied to the distal link on the required motor torque under the same conditions as Fig. 7. The motor torque required for the posture

$$\begin{bmatrix} m_1 g\text{s}_{\theta/2} \\ m_1 g\text{c}_{\theta/2} \\ m_1 g\left(R_\text{J}\text{c}_{\theta/2} + \frac{L_\text{J}}{2}\text{c}_\theta\right) \\ (m_2+m_{\text{ext}})\, g\text{s}_{\theta/2} \\ (m_2+m_{\text{ext}})\, g\text{c}_{\theta/2} \\ (m_2+m_{\text{ext}})\, gR_\text{J}\text{c}_{\theta/2} + m_{\text{ext}}gd_{\text{ext}} \\ T_{03} + m_3 g\text{s}_{\theta/2} \\ m_3 g\text{c}_{\theta/2} \\ T_{03}d_\text{T}\text{c}_{\theta/2} + m_3 g\left(R_\text{J}\text{c}_{\theta/2} + \frac{L_\text{J}}{2}\text{c}_\theta\right) \end{bmatrix} = \begin{bmatrix} 1 & \text{s}_\phi & -1 & -\text{s}_\phi & 0 & 0 & 0 & 0 & -1 \\ 0 & \text{c}_\phi & 0 & -\text{c}_\phi & 0 & 0 & 0 & 0 & 0 \\ 0 & 0 & L_\text{J}\text{s}_{\theta/2} & C & 0 & 0 & 0 & 0 & d_\text{T}\text{c}_{\theta/2} \\ 0 & 0 & 1 & \text{s}_\phi & 0 & 0 & 1 & \text{s}_\phi & 0 \\ 0 & 0 & 0 & \text{c}_\phi & 0 & 0 & 0 & \text{c}_\phi & 0 \\ 0 & 0 & 0 & 0 & 0 & 0 & d_\text{L}\text{c}_{\theta/2} & d_\text{L}\text{s}_{\phi-\theta/2} & 0 \\ 0 & 0 & 0 & 0 & 1 & \text{s}_\phi & -1 & -\text{s}_\phi & 0 \\ 0 & 0 & 0 & 0 & 0 & \text{c}_\phi & 0 & -\text{c}_\phi & 0 \\ 0 & 0 & 0 & 0 & 0 & 0 & L_\text{J}\text{s}_{\theta/2} & C & 0 \end{bmatrix} \begin{bmatrix} f_{01\text{S}} \\ f_{01\text{N}} \\ f_{21\text{S}} \\ f_{21\text{N}} \\ f_{03\text{S}} \\ f_{03\text{N}} \\ f_{23\text{S}} \\ f_{23\text{N}} \\ T_{01} \end{bmatrix} \tag{12}$$

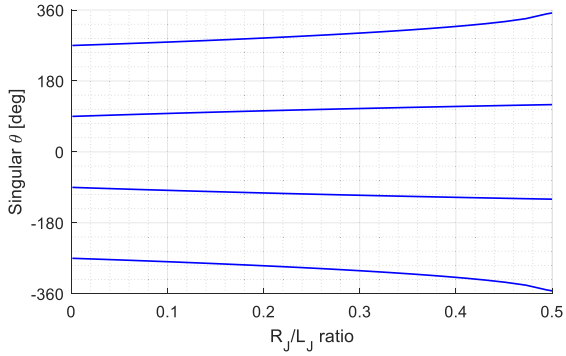


Fig. 9. Change of singular positions affected by $R_{\mathrm{J}}/L_{\mathrm{J}}$ ratio.

of $\theta = 0$ is only $\tau_{\mathrm{M}} = 0.728$ N for $m_{\mathrm{ext}} = 1.0$ kg. Thanks to the effect of speed reduction by the reciprocating cable routing, it is possible to maintain the posture with only considerably low motor torque.

### B. Singular Positions

Unlike in the existing pivot-based parallelograms, the singularities of the proposed mechanism do not exist at $\pm 90^{\circ}$. At singular positions, because $\mathbf{f}_{23\mathrm{S}}$ and $\mathbf{f}_{23\mathrm{N}}$ cannot be determined using (13), the following relation is satisfied:

$$\det \begin{bmatrix} d_{\mathrm{L}}\mathrm{c}_{\theta/2} & d_{\mathrm{L}}\mathrm{s}_{\phi-\theta/2} \\ L_{\mathrm{J}}\mathrm{s}_{\theta/2} & -2R_{\mathrm{J}}\mathrm{c}_{\phi} - L_{\mathrm{J}}\mathrm{c}_{\phi+\theta/2} \end{bmatrix} = 0 \qquad (23)$$

The singular positions of this mechanism that can be obtained are determined by $R_J$ and $L_J$ as follows:

$$\theta = \pm 2\cos^{-1}\frac{-R_{\mathrm{J}} \pm \sqrt{R_{\mathrm{J}}^2 + 2L_{\mathrm{J}}^2}}{2L_{\mathrm{J}}} \qquad (24)$$

As shown in (24), as the radius of the gear constituting the rolling units increases, the distance between the two principal singularities increases and the safe usable driving range of the mechanism increases. However, as shown in Fig. 7, the normal forces on the gears drastically increase at certain angles. This phenomenon is due to the singular positions at which the posture of this mechanism can be unintentionally converted into an anti-parallelogram. Strictly, four singularities, corresponding to the rotation period of this mechanism, are in the 720° range. Fig. 9 shows the singular positions that change according to $R_{\mathrm{J}}/L_{\mathrm{J}}$. As $R_{\mathrm{J}}$ increases, the distance between the principal singularities around $\pm 90^{\circ}$ increases, and they reach $\pm 120.0^{\circ}$ at $R_{\mathrm{J}}/\ L_{\mathrm{J}} = 0.5$.

## V. Experimental Validation

To experimentally confirm that stable wiring is possible in the proposed parallelogram mechanism, the prototype shown in Fig. 10 was first designed. Most of the mechanical components were purchased from MISUMI Korea. A Lugo Labs LUGO Pro 3D printer using PLA material was used to manufacture all the non-standardized components. The wire used in the experiment was a 60227 IEC 53 (H05VV-F) $3 \times 0.75\,\mathrm{mm}^2$ product, widely used for PC power with a 3-core structure and an outer diameter of 6.8 mm. It is sufficiently thick; therefore, it is suitable for checking the wiring influence with the proposed joint mechanism.

To obtain a high reduction ratio and prevent collisions between components, the idlers, which provide the route of the actuation cable, were separated from the central axes of the gears by

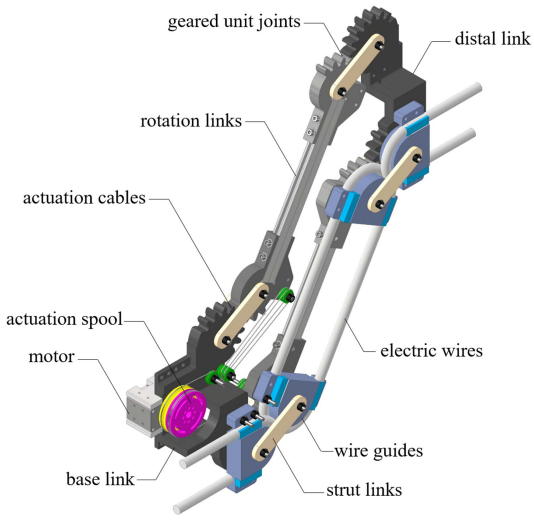


Fig. 10. Prototype design of the proposed parallelogram mechanism.

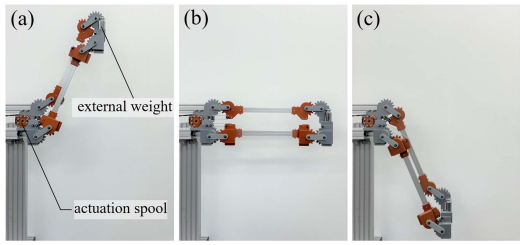


Fig. 11. Vertical actuation with external weight: (a) raised, (b) neutral and (c) lowered positions.

$d_{\mathrm{T}} = 40$ mm. Fortunately, the radius of the gear pitch circle does not affect the normal force transmitted through the gear teeth, but a small gear radius can damage the electrical wires. Therefore, the design of the gear radius should be careful. Generally, the minimum bending radius for winding electrical wires is recommended 8 times the diameter of the conductor. Consequently, in this prototype, a sufficient value of $R_{\mathrm{J}} = 30$ mm was applied by twice the calculated minimum radius. In addition, the length of the rotation links was designed to be $L_{\mathrm{J}} = 300$ mm and reciprocating winding $N_{\mathrm{C}} = 2$ was applied to increase the reduction ratio. The radius of the actuation spool coupled to the motor was $R_{\mathrm{M}} = 25$ mm. The radius of the wire guides was also $R_{\mathrm{G}} = 25$ mm, leaving a 10 mm wide space for wiring between the guides.

The motor was driven five times in a vertical actuation with the ground in the range of $\pm 410^{\circ}$ and the driving torque of the motor was calculated from the input current to the motor. Fig. 11 shows the vertical actuation with external weight applied during the driving experiment with the manufactured prototype. As shown in Fig. 12, a trapezoidal velocity profile for the vertical actuation was applied to the motor control by setting the time for acceleration and constant velocity motion to 0.4 and 8.0 sec, respectively, with a period of 20 sec. The motion in this motor space can be converted into a joint space value using (5), and the driving range of the parallelogram was $\pm 68^{\circ}$. This range is determined by the collision of idlers in the current prototype design, and it is within the singularities of $\pm 97.5^{\circ}$ from (24). Because the maximum rotation speed was only 17.6 deg/sec with low acceleration and velocity, this movement can be regarded as quasi-static. Furthermore, the maximum motor torques required

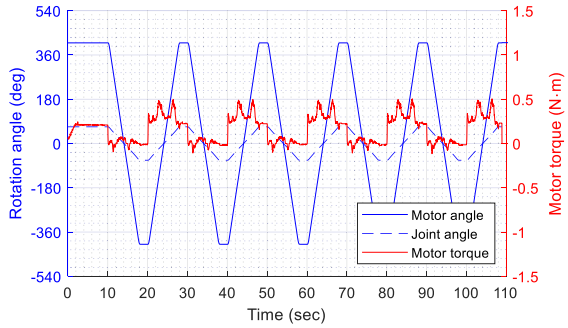


Fig. 12. Measured motor torque for repeated vertical actuation test with external weight 100 g.

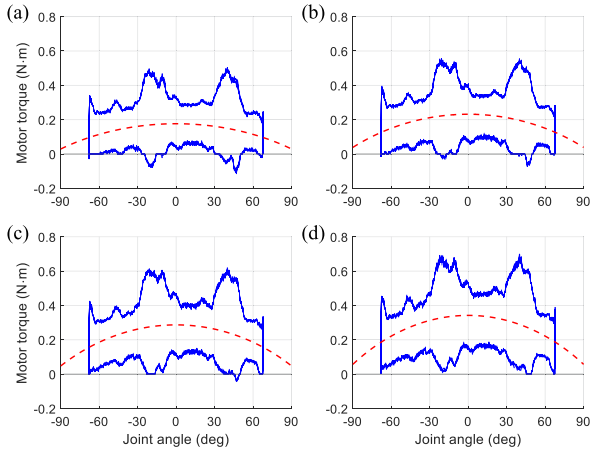


Fig. 13. Measured motor torque for vertical actuation without electrical wires with external weight of (a) 0 g, (b) 100 g, (c) 200 g and (d) 300 g.

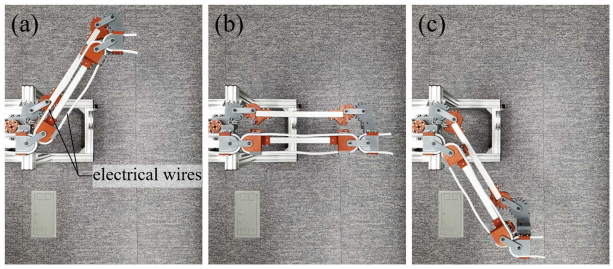


Fig. 14. Horizontal actuation with electrical wires: (a) left, (b) neutral and (c) right positions.

for clockwise and counterclockwise rotations were $-0.0721$ and $0.5551$ Nm, respectively.

The relationship between the rotation link angle and the measured motor torque is depicted in Fig. 13 as blue solid lines for the external weights $m_{\text{ext}} = 0, 100, 2\,00$ and 300 g. The red dotted lines show the theoretically computed motor torque predicted through (18) by applying $m_1 = m_3 = 0.18$ and $m_2 = 0.14$ kg. Here, the resultant Root Mean Square Errors (RMSE) were 0.1845, 0.1808, 0.1851 and 0.1941 Nm, respectively.

In a horizontal actuation experiment, similarly, the motor was repeatedly driven five times in the range of $\pm 410$ degrees, and the driving torque was measured. Fig. 14 shows various postures for the horizontal motion with applied electrical wires, while the relationship between the rotation angle and the measured motor torque is depicted as blue solid lines in Fig. 15. The green dotted line shows the results when the driving speed and acceleration

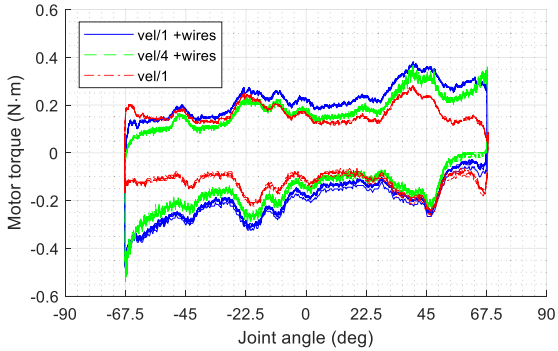


Fig. 15. Measured motor torque for repeated horizontal actuation test.

were reduced by 1/4, and the red dotted line shows another result at the same speed when the electrical wires were removed. For the counterclockwise operation part of the last cycle, the average motor torques required for the three cases were 0.1981, 0.1566 and 0.1156 Nm, respectively.

## VI. Discussion

In the previous vertical actuation experiment, considering the change in the external weight, the resultant RMSEs did not show a significant difference. In the experiment, the torque was indirectly measured using the driving current of the motor, but thanks to the smooth acceleration and deceleration, remarkable peaks in the driving torque were not observed. The torque gap between the upward and downward motion might have been caused by deadband region of motor input current. If using an external torque sensor, the measured torque will be close to the theoretical value, and the torque noise is also expected to be removed.

On the other hand, in the horizontal actuation experiment, the small difference in driving torque according to the driving speed was possibly caused by the rolling friction for the curvature change of the thick wires. In a comparison of cases with and without electrical wires, driving torque did not show a significant difference. This implies that a radius of $R_{\text{G}} = 25$ mm of the circular wire guide was sufficient for easy bending deformation of the wires. During the experiment, wiring was not observed to depart from the planned wiring routes. In addition, except for the first cycle, in which a relatively high torque was measured, the motor torque required to actuate the parallelogram showed fairly high repeatability. Therefore, repetitive and predictable wiring deformation was confirmed to occur because of the stable routing of electrical wires in the proposed parallelogram consisting of rolling units.

From the experimental results, we inferred that the larger the joint angle during a clockwise rotation, the larger the required driving torque tends to be, and the same was also true for counterclockwise rotation. In other words, as shown in Fig. 15, the torque profile measured during unidirectional rotation has a macroscopic positive slope. This is presumed to be because the internal energy for the bending deformation of the wires in the neutral state is minimized. This phenomenon will be reduced if the wire thickness decreases or the radius of the wire guides increases.

However, periodic perturbations were observed in the measured torque during repeated driving, which persisted even when the electrical wires were removed. The dominant peaks of the

long-wave component repeat with a period of approximately $22.5^\circ$.The fact that the spur gears applied for constructing the unit's rolling joints had 16 teeth was not a coincidence. This gear transmission error may cause noise and vibration problems [18]. This long-wave error is presumed to be caused by the imperfect tooth shape of the 3D-printed spur gears. This error can be mitigated by improving the method for manufacturing the gears or by applying helical gears.

The reason for the limited driving range of the prototype in the experiment was the collision between components. A design modification is required to achieve a wider driving range, such as reducing the diameter of the idlers, increasing the radius of the rolling gear $R_{\mathrm{J}}$, and decreasing the distance $d_{\mathrm{J}}$ between the gear axes and idlers. However, caution is needed because this parallelogram may be transposed to an anti-parallelogram at singular positions of approximately $\pm 90^\circ$ unintentionally. As confirmed in Section IV, the application of a large $R_{\mathrm{J}}$ increases the spacing between the principal singularities, and the distal orientation can be stably maintained over a wide range. However, the rotation of this parallelogram is repeated at a cycle of $720^\circ$, and the rotational radius can be significantly reduced at some positions. Therefore, it is necessary to select an appropriate value of $R_{\mathrm{J}}$.

Furthermore, it is necessary to analyze the accuracy and efficiency of the proposed parallelogram mechanism. In the geared unit joint, the strut links might generate gear backlash and result in reduction of rotational accuracy, but the positional and angular errors are estimated to be in the submillimeter and sub-degree range. On the other hand, the efficiency of mechanisms is mainly affected by friction between components. The proposed parallelogram using geared joints can cause more friction than the existing pivot-based joint for the numerous joints, gear trains, and cable-idlers. However, the rotational friction was measured to be less than $0.2\ \mathrm{Nm}$ with small external weights as shown in the vertical experiment. Nonetheless, additional work is needed to accurately measure the accuracy and efficiency of the mechanisms composed of rolling joints and to improve them.

Another important fact confirmed in the force analysis was that, in the interval between $\pm 90^\circ$, the normal forces applied to the gears were not significantly related to the gear radius $R_{\mathrm{J}}$. However, it is necessary to prepare for possible failures in the geared rolling units. Rolamite using flexures or X-joints using an anti-parallelogram, which can transmit a large torque, can be considered as a replacement for the gears [9], [19]. On the other hand, it is required to verify experimentally whether the X-joint mechanism can be applied without modifying the existing cable actuation [20], [21].

Kinematically, when the radius of the gear, $R_{\mathrm{J}}$, is very small, this new gear-based parallelogram can be regarded as an existing pivot-based parallelogram. However, even if $R_{\mathrm{J}}$ is much smaller than the length of the rotation links $L_{\mathrm{J}}$, the distal link position shows a significant difference compared with the pivot-based one. To take advantage of stable wiring, $R_{\mathrm{J}}$ applied to the rolling units must not be significantly reduced. Therefore, the precise kinematic relation derived above is preferred, even if the relative complexity of the calculation increases.

## VII. Conclusion

In this study, the use of geared unit rolling joints was proposed to provide stable wiring to the distal end of robots, and their mechanical characteristics were analyzed. In addition, the effect of the load applied to the distal link on the tangential forces on the gears as well as the singular positions of the parallelogram were analyzed. Furthermore, by manufacturing a parallelogram prototype using geared rolling units, we confirmed that the wiring routes and driving torque showed predictable repeatability even when electrical wires were installed. In conclusion, the proposed parallelogram structure has the advantages of easy addition and modification of wires. Therefore, the proposed rolling joint structure is expected to serve as a new alternative for designing robots.

## References


[1] J. S. Carlson, J. Kressin, T. Hermansson, R. Bohlin, M. Sundbäck, and H. Hansson, "Robot station optimization for minimizing dress pack problems," *Procedia Cirp*, vol. 44, pp. 389–394, May 2016.

[2] S. Iwamura, Y. Mizukami, T. Endo, and F. Matsuno, "Cable-path optimization method for industrial robot arms," *Robot. Comput.-Integr. Manuf.*, vol. 73, 2022, Art. no. 102245.

[3] C. Kaiser and R. Slatter, "Hollow-shaft actuators for intelligent automation," in *Proc. Motion Control Intell. Automat.*, 1992, pp. 107–112.

[4] F. Aghili, M. Buehler, and J. M. Hollerbach, "Design of a hollow hexaform torque sensor for robot joints," *Int. J. Robot. Res.*, vol. 20, no. 12, pp. 967–976, Dec. 2001.

[5] U. Hagn et al., "The DLR MIRO: A versatile lightweight robot for surgical applications," *Ind. Robot: Int. J.*, vol. 35, no. 4, pp. 324–336, 2008.

[6] S. Rader, L. Kaul, P. Weiner, and T. Asfour, "Highly integrated sensor-actuator-controller units for modular robot design," in *Proc. IEEE Int. Conf. Adv. Intell. Mechatronics*, 2017, pp. 1160–1166.

[7] M. Isaksson, G. Clement, and M. Kristan, "An introduction to utilising the redundancy of a kinematically redundant parallel manipulator to operate a gripper," *Mechanism Mach. Theory*, vol. 101, pp. 50–59, Jul. 2016.

[8] Y. J. Kim, S. Cheng, S. Kim, and K. Iagnemma, "A stiffness-adjustable hyperredundant manipulator using a variable neutral-line mechanism for minimally invasive surgery," *IEEE Trans. Robot.*, vol. 30, no. 2, pp. 382–395, Apr. 2014.

[9] J. w. Suh, K. y. Kim, J. w. Jeong, and J. j. Lee, "Design considerations for a hyper-redundant pulleyless rolling joint with elastic fixtures," *IEEE/ASME Trans. Mechatron.*, vol. 20, no. 6, pp. 2841–2852, Dec. 2015.

[10] J. Suh, "Utilization of 2N + 1 units for 2-dof discrete bending joint to transmit perfect axial rotation for laparoscopic instruments," *Int. J. Control, Automat. Syst.*, vol. 18, pp. 186–195, Nov. 2020.

[11] Y. J. Kim, "Anthropomorphic low-inertia high-stiffness manipulator for high-speed safe interaction," *IEEE Trans. Robot.*, vol. 33, no. 6, pp. 1358–1374, Dec. 2017.

[12] W. Li, Y. Wang, S. Togo, H. Yokoi, and Y. Jiang, "Development of a humanoid shoulder based on 3-motor 3 degrees-of-freedom coupled tendon-driven joint module," *IEEE Robot. Automat. Lett.*, vol. 6, no. 2, pp. 1105–1111, Apr. 2021.

[13] S. Pang, W. Shang, F. Zhang, B. Zhang, and S. Cong, "Design and stiffness analysis of a novel 7-dof cable-driven manipulator," *IEEE Robot. Automat. Lett.*, vol. 7, no. 2, pp. 2811–2818, Apr. 2022.

[14] B. Zhao and C. A. Nelson, "Decoupled cable-driven grasper design based on planetary gear theory," *J. Med. Devices*, vol. 7, no. 2, Jun. 2013, Art. no. 020918.

[15] J. J. Craig, *Introduction to Robotics: Mechanics and Control*. London,U.K.: Pearson Educ., 2005.

[16] C. L. Collins, "Kinematics of robot fingers with circular rolling contact joints," *J. Robot. Syst.*, vol. 20, no. 6, pp. 285–296, Jun. 2003.

[17] J. Suh, J. Lee, and D. Kwon, "Underactuated miniature bending joint composed of serial pulleyless rolling joints," *Adv. Robot.*, vol. 28, no. 1, pp. 1–14, Jan. 2014.

[18] A. Palermo, L. Britte, K. Janssens, D. Mundo, and W. Desmet, "The measurement of gear transmission error as an NVH indicator: Theoretical discussion and industrial application via low-cost digital encoders to an all-electric vehicle gearbox," *Mech. Syst. Signal Process.*, vol. 110, pp. 368–389, 2018.

[19] V. Muralidharan and P. Wenger, "Optimal design and comparative study of two antagonistically actuated tensegrity joints," *Mechanism Mach. Theory*, vol. 159, 2021, Art. no. 104249.

[20] Y. J. Kim, J. I. Kim, and W. Jang, "Quaternion joint: Dexterous 3-DOF joint representing quaternion motion for high-speed safe interaction," in *Proc. IEEE/RSJ Int. Conf. Intel. Robot Syst.*, 2018, pp. 935–942.

[21] B. Wang, T. Zhang, and J. Chen, "A modular cable-driven humanoid arm with anti-parallelogram mechanisms and Bowden cables," *Front. Mech. Eng.*, vol. 18, no. 3, Mar. 2023, Art. no. 6.